Liquid Crystals
Publication details, including instructions for authors and subscription information:
http://www.informaworld.com/smpp/title~content=t713926090

Side chain liquid crystal polymers observed by transmission electron microscopy: Microstructure of polymethacrylates and a polyacrylate

V. Tournier-lasserve; A. Boudet; P. Sopéna

To cite this Article Tournier-lasserve, V. , Boudet, A. and Sopéna, P.(1995) 'Side chain liquid crystal polymers observed by transmission electron microscopy: Microstructure of polymethacrylates and a polyacrylate', Liquid Crystals, 19: 4, 433 — 440
To link to this Article: DOI: 10.1080/02678299508032004
URL: http://dx.doi.org/10.1080/02678299508032004

LIQUID CRYSTALS, 1995, VOL. 19, NO. 4, 433–440

Side chain liquid crystal polymers observed by transmission electron microscopy: Microstructure of polymethacrylates and a polyacrylate

by V. TOURNIER-LASSERVE, A. BOUDET* and P. SOPÉNA
CEMES-CNRS, 29 rue Jeanne Marvig, B.P. 4347, F-31055 Toulouse Cedex, France

(*Received 26 June 1994; in final form 1 April 1995; accepted 11 April 1995*)

The smectic structures of three side chain liquid crystal polymethacrylates (PMA) with different terminal groups and a polyacrylate (P_8) were analysed by transmission electron microscopy. Using low electron doses, we were able to obtain diffraction patterns and high resolution (HREM) images from highly oriented undamaged specimens. The results are compared with those from previous X-ray diffraction experiments. All the polymers have a smectic A structure. The PMA and P_8, each with a CN terminal group, are the least ordered. Their diffraction patterns show a smectic A_d structure. PMA-OC_4H_9 and PMA-ϕ have smectic A_1 structures. The smectic layers, seen by high resolution images, are very well oriented with only a few defects such as notches or kinks. In the A_d structure, the well-ordered domains are smaller, and the defects are more numerous. The differences are due to the influence of the polarization of the side chain terminated with CN.

1. Introduction

The structure of side chain liquid crystal polymers results from the competition between the tendency towards liquid crystalline order due to the mesogenic core and the tendency towards statistical disorder due to the polymeric chain. These are more or less related by the flexible spacer that links the mesogenic core to the chain. A fourth element plays a role: the terminal group attached at the end of the side chain. Several authors have therefore studied these structures and the influence of these elements: nature of the mesogenic core, nature of the chain, length of the spacer, nature of the terminal group [1, 2].

In this paper, we study three polymers that have the same main chain—polymethacrylate (PMA)—, the same mesogenic core and spacer, and differ in the terminal group $-OC_4H_9$, $-C_6H_5$, or $-CN$. We shall refer to them as PMA-OC_4H_9, PMA-ϕ and PMA-CN, respectively. The differences in their structures will therefore be due to the terminal group.

The common ways of characterization of such polymers are differential scanning calorimetry (DSC) and optical microscopy. By X-ray diffraction, Davidson *et al.* [3], obtained more precise results. They oriented the specimens in a magnetic field and could detect the smectic A–nematic transitions of PMA-OC_4H_9, PMA-ϕ and PMA-CN. The last two had not previously been studied by DSC and optical microscopy.

We also study here the cyano-substituted mesogenic side chain polyacrylate referred to as P_8. Its characteristics were reported in [4] by Davidson *et al.*

Transmission electron microscopy (TEM) has seldom been used to observe side chain liquid crystal polymers. Like all polymers, they suffer radiation damage under the electron beam and their observation is possible only at moderate magnifications under low dose conditions [5, 6]. High resolution electron microscopy (HREM) images can be obtained only for beam resistant polymers [7]. Voigt Martin *et al.* [8–11], were able to record high resolution images of two main chain/side chain liquid crystal polymers and of PMA-OC_4H_9. For PMA-OC_4H_9 [8, 9, 12], they observed diffraction patterns specific to a smectic A and sometimes smectic E structures. In HREM, the smectic layers are clearly visible in limited domains. For the two main chain/side chain liquid crystal polymers, the smectic layers are also visible by HREM and some edge dislocations have been detected.

In these papers, the specimens were dissolved, floated on a water surface and annealed on a microscope grid. In this paper, we intend to study highly ordered structures, and for this purpose, the specimens were strongly oriented by a magnetic field.

The electron diffraction patterns of the four polymers are depicted and compared in § 3. Finally, the fine details of the smectic structure are examined by HREM. HREM

* Author for correspondence.

0267–8292/95 $10·00

images of the smectic layers have been obtained for PMA-OC_4H_9, PMA-ϕ and P_8. This aspect is described and discussed in § 4.

2. Experimental

2.1. *Materials*

The three mesomorphic polymethacrylates that we have studied differ only in the end group (*R*) of the side chain. Their molecular structures are given in figure 1. These side chain liquid crystal polymers were synthesized by Keller [3]. The degree of polymerization is about 500, and the polymer is obtained in the form of a powder [3]. The phase transition temperatures (see table 1) have been determined by differential scanning calorimetry (DSC), optical observations and checked by X-ray diffraction, as already reported in [3]. At room temperature, the specimens are in their glassy smectic A state.

The cyano-substituted side chain mesomorphic polyacrylate P_8, the molecular structure of which is given in figure 1, has been synthesized by Davidson *et al.* [4]. The degree of polymerization is about 30. The phase transition temperatures are reported in table 1. For this polymer, the glass transition temperature is slightly below room temperature.

PMA-R :

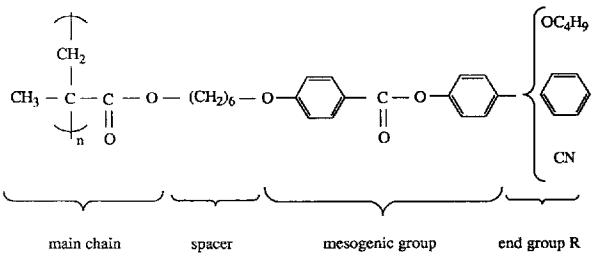

P_8 :

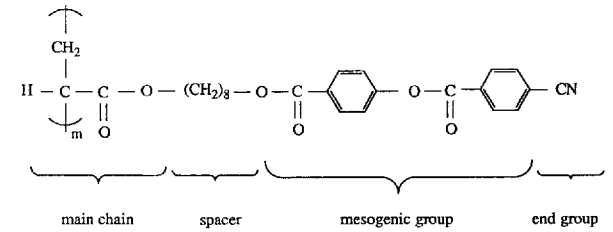

Figure 1. Molecular structures of the three side chain liquid crystal polymethacrylates referred to as PMA-*R* and the polyacrylate P_8.

Table 1. Phase transition temperatures (°C) of the polymers. T_g: glass transition temperature. S_A: smectic A; N: nematic; I, isotropic liquid.

Polymer	T_g	Transition temperatures
PMA-OC_4H_9	50	S_A 95 N 110 I
PMA-ϕ	67	S_A 150 N 173 I
PMA-CN	50	S_A 96 N 108 I
P_8	15	S_A 110 I

As in the previous study by X-ray diffraction, the specimens were prepared as small cylindrical blocks oriented by a magnetic field in order to have a well-ordered structure throughout the volume of the sample. This alignment was achieved inside the X-ray diffractometer by applying a 1·7 T magnetic field throughout the thermal process, so that the degree of alignment could be followed by X-ray diffraction. The powder was put in a Lindemann glass tube 1·5 mm in diameter, inserted in the diffractometer and subjected to the magnetic field **B** perpendicular to the tube axis. The specimens were submitted to a thermal cycle (see figure 2), comprising a stage in the isotropic state, and then a stage in the nematic domain (or smectic for P_8) where the mesogenic cores can orientate themselves along the **B** direction. The cooling rate was very low to ensure that the time spent in the nematic phase (or smectic) is long enough for the specimen to reach equilibrium. This was more difficult to achieve in the case of PMA-CN and P_8. The specimen obtained is a nearly transparent homogeneous cylinder. The mesogenic cores are aligned along the magnetic field and the smectic layers lie parallel to the cylinder axis (figure 3).

2.2. *Sample preparation for transmission electron microscopy*

To be suitable for TEM observations, the samples must be as thin as 0·2 μm or less. Since our purpose was to study specimens already subjected to an ordering treatment in the X-ray diffractometer and without adding any further process, the specimens were sectioned in thin slices by ultramicrotomy. The ultramicrotome was operated with a diamond knife at room temperature. Sectioning of the cylinder was achieved in a plane perpendicular to the cylinder axis (see figure 3) so that the mesogenic cores lie in the section and the smectic layers are perpendicular to the section. This could be controlled only within the small inaccuracy of the sample position during sectioning. The sections were retrieved on carbon coated grids and

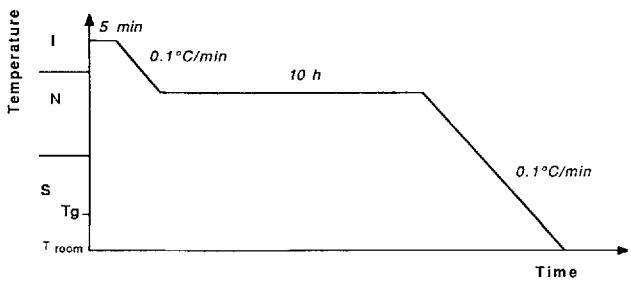

Figure 2. Thermal processing of the polymethacrylates.

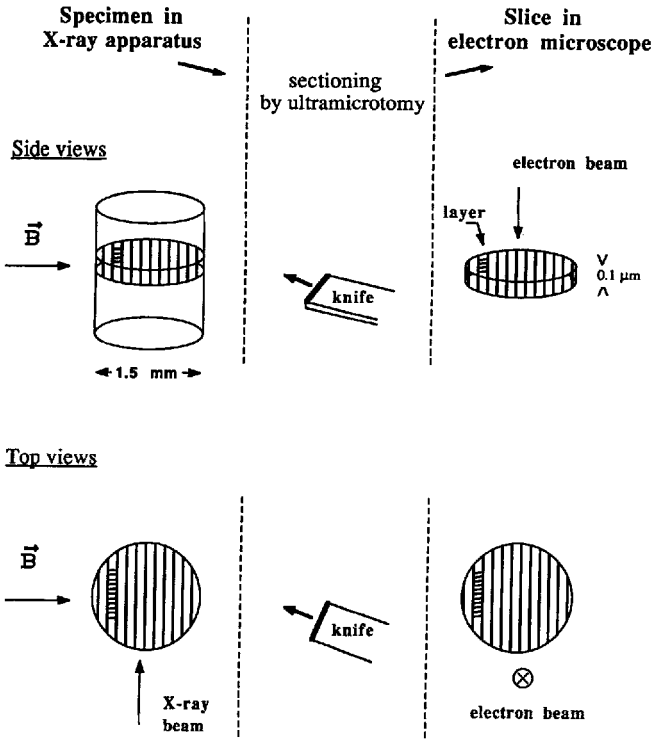

Figure 3. Comparison of the geometry of the specimen in the X-ray apparatus (left) and, after sectioning, in the electron microscope (right). Upper part: side views; lower part: top views. **B**: magnetic field direction.

observed by TEM. As can be seen in figure 3, the electron beam, like the X-ray beam, is parallel to the smectic layers, so that diffraction patterns are equivalent.

In another paper [13], we have reported the mechanical effect due to the knife compression during sectioning. This resulted in a tilt of the side chains by an angle up to 10° from the original 90° position. This tilt angle was dependent on the layer orientation with respect to the knife edge.

In the same paper, we reported that when the sections are subsequently annealed on the grids for two days at a temperature below the smectic A–nematic (or isotropic for P_8) transition, then slowly cooled at 1°C min^{-1} down to room temperature, the normal orientation of the side chains is recovered. Moreover, the characteristics of the features in the diffraction pattern (Bragg spots and crescents) are similar to those on non-annealed sections, in particular the extension of the crescents is unchanged [13]. Consequently, we analyse the electron diffraction on annealed sections. However, annealing has been found to introduce a small number of additional defects in the layers visible on high resolution images, while the layers are well preserved in non-annealed specimens. Therefore high resolution images were obtained on non-annealed sections.

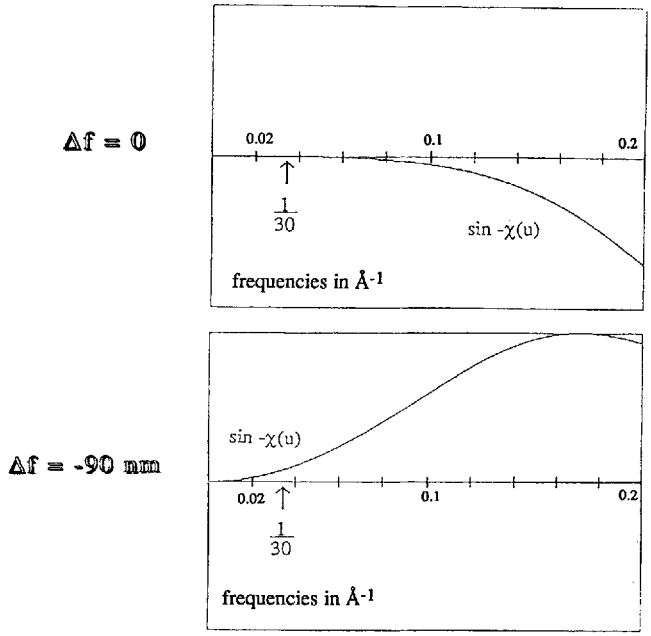

Figure 4. Transfer functions of the microscope at 200 kV for $\Delta f = 0$ and $\Delta f = -90$ nm showing the intensity versus the spatial frequency u. The $\frac{1}{5}$ to $\frac{1}{30}$ Å^{-1} frequencies are enhanced by defocusing at -90 nm.

2.3. *Observation conditions*

All the observations were made with a Philips CM20 microscope operated at 200 kV. The smectic structure was investigated by electron diffraction on local areas as small as 6 μm in diameter and by high resolution microscopy. The term 'high resolution' means that the image is obtained by the interference of two symmetric diffracted beams, even if the lattice periodicity is large (30 Å). The principal difficulty comes from the radiation damage due to the electron beam, which destroys the order. To limit this damage, micrographs were recorded at low dose and we used a specimen holder cooled by liquid nitrogen. For high resolution imaging, the specimen was deposited on holey carbon film to minimize the background noise. According to Johnson [14], the contrast of the lattice can be improved by enhancing spatial frequencies that are about four times smaller than the lattice spacing. In our case, a Scherzer defocus equal to -90 nm enhances the 7–8 Å range, and the 20–30 Å range is also increased (see figure 4).

3. Influence of the terminal group on the smectic A microstructure

The diffraction patterns of the four types of sample, schematized in figure 5, are similar and typical of a smectic A structure. They are composed of four elements, the characteristics of which are given in tables 2 and 3. Three of them are analogous to the X-ray diffraction patterns [3, 4]: small equidistant Bragg spots (*a*) aligned along the meridian, diffuse crescents (*b*) centred on the equator, and

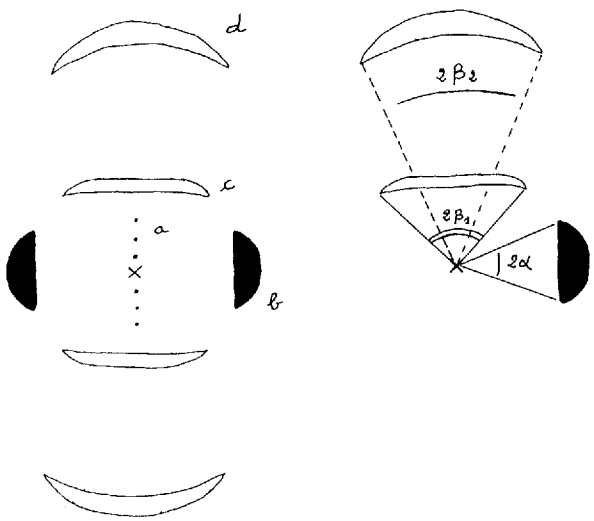

Figure 5. Diagram of a typical electron diffraction pattern. (*a*) Bragg spots; (*b*) diffuse crescents; (*c*) diffuse lines for PMA-OC_4H_9 and PMA-ϕ; (*d*) diffuse arcs. On the right, definition of the angles α, β_1, β_2.

diffuse lines (*c*). We also see a fourth element, the diffuse arcs (*d*), that has not been observed by X-ray diffraction [3].

The intense fine spots (*a*) are due to Bragg scattering at the smectic layers. The number of spots (*a*) in PMA-OC_4H_9 is a little larger than in PMA-ϕ and PMA-CN, implying that its order is better. This difference had not been observed in X-ray diffraction patterns.

The width of the crescents and their position at right angles to the line of the Bragg spots are indicative of a smectic A structure. The mean distances between the side chains, deduced from the crescent radius (see table 2) are the same for all four samples.

The periodicity *d* of the layers, deduced from the periodicity of the Bragg spots within an inaccuracy given by the width of the spots (see table 2) was compared to the length *l* of the side chains (see figure 6). The lengths *l* for the PMAs, including a CH_3 group representing the main chain, were estimated with the aid of an optimized model of the molecules, obtained by a molecular mechanics calculation. The length of the polyacrylate P_8 side chain, evaluated by a Dreiding stereomodel, has been taken from [4].

In PMA-OC_4H_9, *d*/*l* is equal to 1, and the side chains are packed at the same level inside the layers, with no shift along the normal to the layers **n** (smectic A_1 structure, see figure 6). In PMA-ϕ, *d*/*l* is a little higher than 1 (= 1·1), indicating that the side chains are a little shifted with respect to one another along **n**. The packing is thus less compact than in PMA-OC_4H_9. The cause of the variations in *d*/*l*, and of the modification of the side chain packing is to be sought in the difference between the terminal groups. The replacement of the flexible OC_4H_9 end group by the rigid ϕ has made it more difficult for the side chains to match one another.

The nitrile group CN has a still stronger influence. Its polarity causes the chains to pack in an almost double layer arrangement (smectic A_d structure, see figure 6). In PMA-CN (*d*/*l* = 1·5), the side chain packing is the least compact of the three polymethacrylates. It gives more chance for main chain winding. Small angle neutron scattering experiments by Noirez *et al.* [15], have shown that the main chain is excluded from the side chain packing, and according to Leadbetter *et al.* [16], side chains attached to a main chain lying above and others attached to a main chain lying below (see figure 6) are juxtaposed in the same layer. The up and down side chains partially overlap by 10 Å. In P_8, which also has the CN end group (see figure 1), the same effect is observed: the ratio *d*/*l* (= 1·7), higher than in PMA-CN, is indicative of a still less compact arrangement. The overlap of the up and down side chains is now only 8 Å.

The differences in the packing of the side chains in the

Table 2. Characteristics of the Bragg spots (*a*) and the crescents (*b*). *d*: Periodicity of the layers, *l*: length of the side chain given by molecular energy optimization for the three polymethacrylates and by a Dreiding stereomodel for the polyacrylate P_8 [4]. The lateral mean distance between the side chains is deduced from the radius of the crescent. 2α: Extension angle of the crescents defined in figure 5.

	Polymer			
Parameter	PMA-OC_4H_9	PMA-ϕ	PMA-CN	P_8
Bragg spots shape	Spots	Spots, sometimes small arcs	Spots	Spots
Number of visible orders	3	2	2	3
d/Å	28·7 ± 0·9	29·6 ± 0·9	35·9 ± 1·2	48 ± 2
l/Å	27·8	25·9	23·1	28
d/*l*	1·03	1·1	1·5	1·7
	S_{A_1}	S_{A_1}	S_{A_d}	S_{A_d}
Side chain lateral distance/Å	4·5 ± 0·4	4·5 ± 0·4	4·5 ± 0·4	4·45 ± 0·4
2α/degree	30–40	30–40	70	80

Table 3. Characteristics of the diffuse lines (*c*) and diffuse arcs (*d*). *h*: Characteristic distance deduced from the distance of the line (*c*) to the central beam; $2\beta_1$ and $2\beta_2$: lateral extensions of the lines and diffuse arcs (cf. figure 5).

Parameter	Polymer			
	PMA-OC_4H_9	PMA-ϕ	PMA-CN	P_8
Characteristic distance *h* of the diffuse lines (*c*)/Å	5·75	5·3	—	—
$2\beta_1$/degree	~80	~70	—	—
Characteristic distance of the diffuse arcs (*d*)/Å	2·09	2·09	2·09	2·09
$2\beta_2$/degree	40–45	40–45	40–45	80

A_l and A_d structures are also reflected in the crescents (*b*) and in the diffuse lines (*c*) of the diffraction patterns. The crescents are well defined and intense for PMA-OC_4H_9, a little less intense for PMA-ϕ, and more diffuse for PMA-CN and P_8. Their extension (angle 2α, see figure 5), is representative of the tilt range of the side chains, distributed around the normal **n**. This is higher for PMA-CN and P_8 than for PMA-OC_4H_9 and PMA-ϕ. This means that in the A_d structure, where the arrangement of the side chains is less compact, the side chains have a greater freedom to be disorientated. The two diffuse lines (*c*) centred on the meridian are visible in PMA-OC_4H_9 and PMA-ϕ, and related to a distance *h* around 5–6 Å (see table 3). This indicates an order on a smaller scale that does not exist in the A_d structures of PMA-CN and P_8.

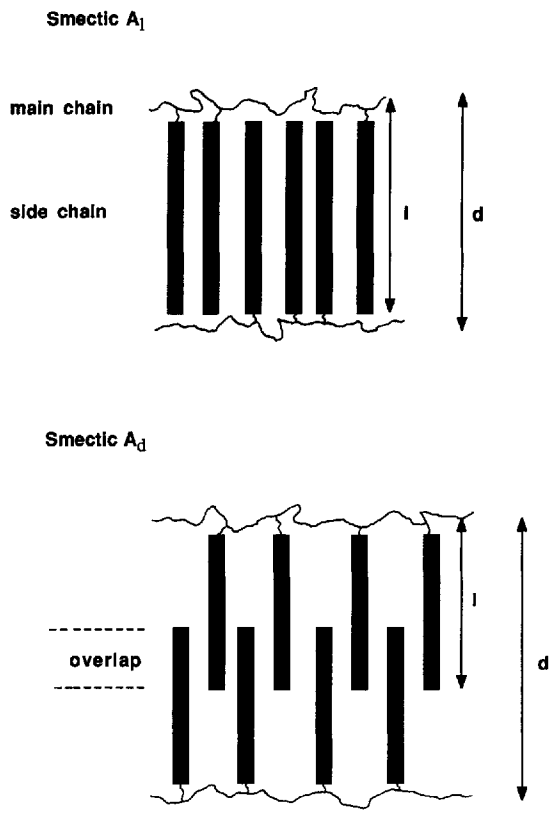

Figure 6. Sketch of the organization of the side chains and main chain of PMA-OC_4H_9 (smectic A_l) and PMA-CN (smectic A_d).

The two diffuse arcs (*d*) centred on the meridian are faint, and hardly visible, and it is difficult to measure their characteristics. They correspond to the same distance for the four samples, about 2·1 Å, and are related to the side chains (see table 3). This is supported by the fact that the diffuse arcs become tilted in the same manner as the crescents (*b*) during sectioning [13], keeping at right angles to each other. They seem to be due to some internal part of the mesogenic core. The diffuse arcs (*d*) were not detected in the X-ray diffraction patterns because the distance 2·1 Å lies out of their field.

We expected to see differences between the electron diffraction, obtained from tiny domains in thin slices of the cylinder, and the X-ray diffraction obtained from the whole cylinder before sectioning [3]. The X-ray pattern is the sum of local orientations of the small domains analysed by electron microscopy. Instead of being different, it is noticeable that the electron diffraction pattern is similar to the X-ray pattern. This means that, with the aid of the magnetic field, the same local orientation of the molecules has been extended to the whole volume of the specimen. Its microstructure represents an outstandingly well-oriented smectic A phase.

For that reason, it was possible to form HREM images and study the microstructure on the scale of the smectic layers, as described in § 4.

4. Defects in the smectic layers

By selecting the spots (*a*) to form the image, we have succeeded in visualizing the smectic layers (see figures 7 and 8). The lines are in fact interference fringes. They represent the diffracting layers seen edge-on. High resolution images of highly ordered smectics are very useful, because it is possible to see and analyse the disposition of the smectic layers. Our purpose was to investigate this disposition and to look for eventual defects.

This could be achieved only in non-annealed sections, as shown in a previous paper [13]. Although in annealed

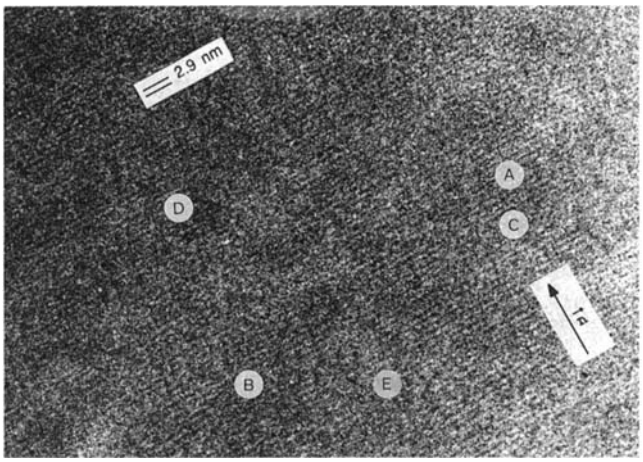

(*a*)

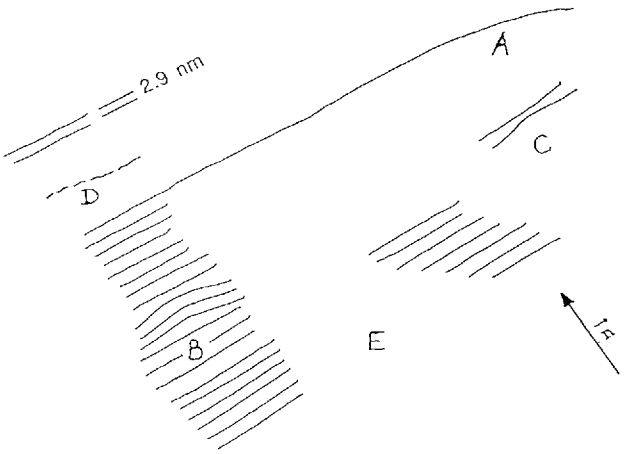

(*b*)

Figure 7. (*a*) High resolution image of the smectic layers in PMA-OC_4H_9. (*b*) Sketch of figure (*a*) showing the defects of the fringes. (*A*) small curvature; (*B*) notch; (*C*) sinuosity; (*D*) dots; (*E*) loss of contrast.

sections the side chains are again organized in a smectic A structure, and the layers are well oriented, the condition of alignment imposed by the magnetic field has been relaxed, so that many defects have been introduced with respect to the non-annealed sections. The analysis of these non-annealed sections is instructive if we keep in mind that the side chains have been slightly tilted.

High resolution images were obtained only in very well-oriented specimens. For example, it was impossible to form images of PMA-CN specimens because their orientation was not good enough. Results are now reported for PMA-OC_4H_9, PMA-ϕ and P_8.

4.1. *PMA-OC_4H_9*

The layers in PMA-OC_4H_9 are clearly visible over large domains where they are stacked in piles of up to 350 layers (see figure 7 (*a*)). This packing is very regular and extends through micrometre long domains. The length of the layers is about 200 nm. They are straight over 100 nm, with only a small curvature (*A*, figure 7 (*a*), (*b*)), usually less than 5° but sometimes a little more, up to 10°, which corresponds to a curvature radius of 0·8 μm.

We could not detect any edge dislocations. Some other rare defects are visible (see figure 7 (*a*), (*b*)). These are either notches, or irregularities in the spacing, or loss of contrast. The notches (*B*) are small local bumps or

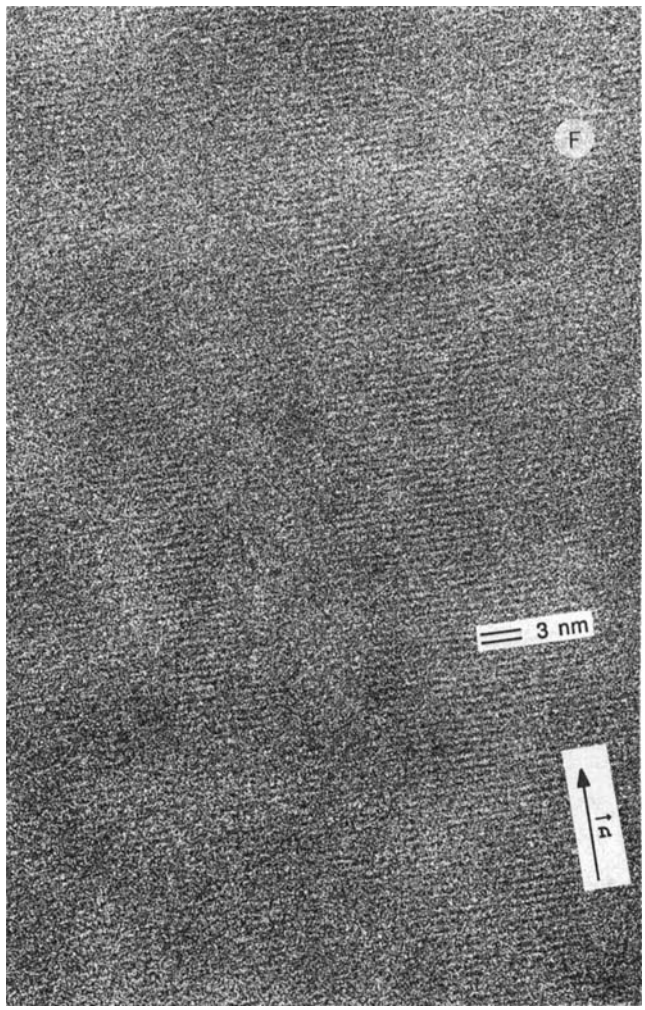

(*a*)

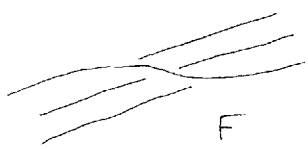

(*b*)

Figure 8. (*a*) High resolution image of the smectic layers in PMA-ϕ. (*b*) Sketch of the kink (F) in figure (*a*).

'detours' of a fringe, disturbing 1 or up to 5 layers (curvature radius about 28 nm). Some layers are locally more sinuous, so that the distance between successive fringes does not remain constant (*C*). These irregularities affect only small areas, no longer than 20 nm, and do not disturb the adjoining layers.

Sometimes, there is a loss of contrast of the fringe, which resembles a dotted zigzag line (*D*). This loss of contrast is either seen as small defects in the fringe or extends over a large area between the well contrasted fringe domains (*E*).

4.2. *PMA-ϕ*

The smectic layers in PMA-ϕ are also clearly visible in domains (see figure 8 (*a*)), the dimensions of which are about 60 nm along the fringe direction and more than 400 nm in the perpendicular direction (about 130 layers). The fringes are therefore shorter than the PMA-OC_4H_9 fringes, and their contrast is also lower. Some notches and many local sinuosities are present. The most common defects are kinks of the fringes, in which the fringe bends in an oblique direction, then joins the next fringe or sometimes a fringe two or three layers further on (see figure 8 (*a*), (*b*), *F*). No additional or missing fringes (no edge dislocations) could be found.

In contrast to PMA-OC_4H_9, no curvature of the layers over a long distance is visible. The change of orientation, evidenced by the slight extension of the Bragg spots in the diffraction patterns, is achieved by locally identified defects, like the detours B, and especially the kinks F. These kinks could be interpreted as screw dislocations, if we imagine that a part of the film was cut along a layer, then one of the lips was slipped over the other. In this case, the thickness would be double over this area, and a contrast would appear, but it does not. Furthermore, to fit the disorientation, several kinks would be produced, and we observe only isolated ones. In fact, high resolution contrast in a defect is difficult to analyse, since it is an interference contrast. Only simulation of precise models can generate confidence in its interpretation.

4.3. *Polyacrylate P_8*

Since P_8 has a less compact structure than PMA-CN, we did not expect to obtain HREM images. However, this has been possible because P_8 could be better oriented by the magnetic field. The contrast of the fringes is lower than in the two smectic A_1 polymethacrylates, and the micrographs are difficult to print in an article. The smectic domains observed in this A_d structure are smaller. In some areas, the layers are straight and visible over 100 nm. Some estimations from X-ray diffraction patterns [17] had predicted a population of edge dislocations with a density of $10^8\,cm^{-2}$. This corresponds to a probability of 1 in 30 of observing one in a surface equivalent to the picture in figure 8. No edge dislocation could in fact be detected.

However, other parts are more disordered and full of defects. These domains display local loss of contrast in many places and short bent fringes (about 25 nm). The mean direction of the fringes varies over 20–30° from one domain to the other. It is possible that the system is mechanically disturbed during the ultramicrotomy that is carried out at room temperature, slightly above the glass transition. In response to this stress, the system prefers to match the variations of the director by local disorientations, rather than by a soft progressive curvature of the layers as in PMA-OC_4H_9. These disorientations could be favoured by the A_d structure which is less compact than the A_1 structure (cf. § 3), and thus more compressible. But the low degree of polymerization of P_8 could also play a role. We could not obtain a measurement of the gyration radius of the main chain along the layers. However, since it is about 10 nm in PMA-OC_4H_9 according to neutron scattering experiments, and since the degree of polymerization is 16 times smaller, this gyration radius should be approximately 2·5 nm. This is very low (equal to the side chain length), and there should be little transverse cohesion in the main chain sub-layer. The zones where different main chains are in contact could act as points of possible defects.

5. Conclusions

Despite the electron radiation damage undergone by the polymers, transmission electron microscopy has proved to give interesting information relevant to the investigation of their structure. The local structure exhibited by electron diffraction patterns could be compared with the global X-ray diffraction pattern, and high resolution images provided evidence for the detailed disposition of the smectic layers.

According to the analysis of the electron diffraction, all three polymethacrylates and the polyacrylate are very well oriented throughout the whole specimen. This is due to the efficiency of the magnetic field applied during the thermal process. To keep this oriented structure, the specimens were cut by ultramicrotomy. High resolution images confirm this ordered structure on a small scale, and show that very few defects are present, and in particular no edge dislocations.

The comparison of the structures of the three mesomorphic polymethacrylates, differing only in their terminal groups, reveals some differences attributed to the influence of the terminal group. With respect to PMA-OC_4H_9 and PMA-ϕ, the polymers PMA-CN and P_8 exhibit a less ordered structure.

PMA-OC_4H_9 has the most ordered structure with large well-oriented domains and some rare defects. PMA-ϕ is

a little less ordered. The fringe domains are smaller and the fringes are more often locally curved. More defects appear inside, especially kinks. These two polymers have a smectic A_1 structure, but the packing of the side chains is less compact in PMA-ϕ ($d/l = 1{\cdot}1$). The replacement of the terminal group OC_4H_9 by phenyl confers more rigidity to the side chains, reduces their freedom to adopt a position close to the other neighbouring chains, and leaves more defects in the layer disposition.

PMA-CN is still more disordered with its smectic A_d structure. This can be attributed to the influence of the CN group, and the subject polarization of the side chain. The same influence has been found in the polyacrylate P_8. In this polymer, domains with short curved fringes and local loss of contrast could be due to the deformation undergone during ultramicrotomy. The A_d structure and the low molecular mass could favour the appearance of defects.

We thank P. Davidson and P. Keller for providing us with specimens and for many helpful discussions and advice. We also thank J. Devillers for help with the molecular mechanics calculation.

References

[1] PERCEV, V., and PUGH, C., *Side Chain Liquid Crystal Polymers*, edited by McArdle (Chapman & Hall), Chap. 3.
[2] FINKELMANN, H., *Side Chain Liquid Crystal Polymers*, edited by McArdle (Chapman & Hall), Chap. 2.
[3] DAVIDSON, P., KELLER, P., and LEVELUT, A. M., 1985, *J. Phys. France*, **46,** 939.
[4] DAVIDSON, P., and STRZELECKI, L., 1988, *Liq. Crystals*, **3,** 1583.
[5] BOUDET, A., 1986, *J. Phys. France*, **47,** 1043.
[6] BOUDET, A., and KUBIN, L. P., 1982, *Ultramicroscopy*, **8,** 409.
[7] BOUDET, A., MARTIN, D. C., and THOMAS, E. L., 1987, *Proceedings of European Symposium on Polymer Material, European Polymer Federation*, Lyon–France, ECO5.
[8] DURST, H., and VOIGT-MARTIN, I. G., 1986, *Makromolek. Chem. rap. Commun.*, **7,** 785.
[9] VOIGT-MARTIN, I. G., and DURST, H., 1987, *Liq. Crystals*, **2,** 601.
[10] VOIGT-MARTIN, I. G., and DURST, H., 1989, *Macromolecules*, **22,** 168.
[11] VOIGT-MARTIN, I. G., KRUG, H., and VAN DYCK, D., 1990, *J. Phys. France*, **51,** 2347.
[12] VOIGT-MARTIN, I. G., and DURST, H., 1987, *Liq. Crystals*, **2,** 585.
[13] TOURNIER-LASSERVE, V., BOUDET, A., and SOPÉNA, P., 1995, *Ultramicroscopy*, **58,** 123.
[14] JOHNSON, J., and CRAWFORD, D., 1973, *J. Microsc.*, **98,** 313.
[15] NOIREZ, L., MOUSSA, F., COTTON, J. P., KELLER, P., and PÉPY, G., 1991, *J. stat. Phys.*, **62,** 997.
[16] LEADBETTER, A. J., TEMME, F. P., HEIDEMANN, A., and HOWELLS, W. S., 1975, *Chem. Phys. Lett.*, **34,** 363.
[17] DAVIDSON, P., PANSU, B., LEVELUT, A. M., and STRZELECKI, L., 1991, *J. Phys. II*, **1,** 61.